Published in final edited form as:
*Chemosphere*. 2019 April ; 221: 392–402. doi:10.1016/j.chemosphere.2019.01.063.

# Potential utility of graphene-based nano spinel ferrites as adsorbent and photocatalyst for removing organic/inorganic contaminants from aqueous solutions: A mini review

**Chang Min Park**[a], **Young Mo Kim**[b], **Ki-Hyun Kim**[c], **Dengjun Wang**[d], **Chunming Su**[e], **Yeomin Yoon**[f]

[a]Department of Environmental Engineering, Kyungpook National University, 80 Daehak-ro, Buk-gu, Daegu 41566, Republic of Korea

[b]School of Earth Sciences and Environmental Engineering, Gwangju Institute of Science and Technology, 123 Cheomdangwagi-ro, Buk-gu, Gwangju 61005, Republic of Korea

[c]Department of Civil and Environmental Engineering, Hanyang University, 222, Wangsimni-Ro, Seoul 04763, Republic of Korea

[d]National Research Council Research Associate at the U.S. Environmental Protection Agency, 919 Kerr Research Drive, Ada, OK 74820, USA

[e]Groundwater, Watershed and Ecosystem Restoration Division, National Risk Management Research Laboratory, Office of Research and Development, U.S. Environmental Protection Agency, 919 Kerr Research Drive, Ada, OK 74820, USA

[f]Department of Civil and Environmental Engineering, University of South Carolina, Columbia, 300 Main Street, SC 29208, USA

## Abstract

Toxic substances such as heavy metals or persistent organic pollutants raise global environmental concerns. Thus, diverse water decontamination approaches using nano-adsorbents and/or photocatalysts based on nanotechnology are being developed. Particularly, many studies have examined the removal of organic and inorganic contaminants with novel graphene-based nano spinel ferrites (GNSFs) as potential cost-effective alternatives to traditionally used materials, owing to their enhanced physical and chemical properties. The introduction of magnetic spinel ferrites into 2-D graphene-family nanomaterials to form GNSFs brings various benefits such as inhibited particle agglomeration, enhanced active surface area, and easier magnetic separation for reuse, making the GNSFs highly efficient and eco-friendly materials. Here, we present a short review on the state-of-the-art progresses on developments of GNSFs, as well as their potential application for removing several recalcitrant contaminants including organic dyes, antibiotics, and heavy metal ions. Particularly, the mechanisms involved in the adsorptive and photocatalytic degradation are thoroughly reviewed, and the reusability of the GNSFs is also highlighted. This review concludes that the GNSFs hold great potential in remediating contaminated aquatic environments. Further studies are needed for their practical and large-scale applications.

**Keywords**

Graphene; Nano spinel ferrite; Adsorbents; Photocatalysts; Water treatment

## 1. Overview on the removal of organic and inorganic contaminants by graphene-based nano spinel ferrites (GNSFs)

Organic and/or inorganic contamination in water bodies adversely influences the aquatic environment and community health. Much attention has been paid to emerging and persistent organic pollutants particularly for those of endocrine disrupting compounds (EDCs) (*e.g.*, bisphenol A (BPA), metronidazole, and levofloxacin) and many industrial dyestuffs (Park et al., 2017). EDCs are chemical compounds with xenobiotic origins altering vertebrate endocrine systems (Veldhoen et al., 2014), and they are widely detected in natural freshwater near wastewater discharges. EDCs can cause undesired physiological effects in wildlife and human beings at low-level exposure (Archer et al., 2017, Jin et al., 2018). The presence of synthetic dyes in effluents is also a global concern for the environment due to their toxicity, carcinogenicity, and mutagenicity. Those organic contaminants have low biodegradability but high stability toward (photo)chemical treatments due to their complex aromatic structures (Inyang et al., 2014). Aside from organic pollutants, many inorganic compounds such as toxic heavy metals are also among the worst contaminants encountered in aquatic environment, due to their persistence, bioaccumulation/magnification potential, and high toxicity.

Many such contaminants are resistant to conventional treatment processing, such as simple physical, chemical, and biological water decontamination strategies. This issue has led to a recent surge of research interest into developing novel carbonaceous nano-adsorbents and/or photocatalysts using green energy sources (*e.g.*, solar light) for advanced water treatment (Park et al., 2018, Wang et al., 2017a, Xiong et al., 2018, Zhou et al., 2019). Broad applications have been reported for the graphene-family nanomaterials, a family of carbon derivatives with structures similar to graphite, which include (i) graphene (*i.e.*, single-layer sheets of $sp^2$-hybridized carbon network); (ii) graphene oxide (GO) containing carboxyl, carbonyl, epoxide, and hydroxyl functional groups on the basal planes and/or edges; (iii) reduced GO (rGO) with a few oxygen groups, and (iv) few-layer graphene (Al-Hamadani et al., 2018). The graphene-family nanomaterials have exhibited outstanding properties such as high adsorption capacity for organic/inorganic contaminants, electrical conductivity, and mechanical strength (Goodwin et al., 2018, Yi et al., 2018).

After using graphene-family nanomaterials for treatment, a great deal of energy (solid/liquid separations using centrifugation or membrane filtration) is required to recover or reuse them from aqueous solutions (Deng et al., 2010). To resolve these issues, spinel ferrites ($MFe_2O_4$, M = Co, Cu, Zn, Ni, Mn, *etc.*) can be incorporated as core material into graphene-family nanomaterials. $MFe_2O_4$ ferrites are magnetic materials in oxidation states of M(II) and Fe(III) having a face-centered cubic structure. In normal spinel, M(II) and Fe(III) cations occupy tetrahedral and octahedral sites, respectively, while in inverse spinel half of Fe(III) occupy tetrahedral sites. The ferrites have attracted a great deal of interest due to their

remarkable magnetic, catalytic, and electrical properties that are potentially useful for diverse practical applications (Bao et al., 2007). The ferrites display advantageous optical absorption for lower energy photons ($h\nu \sim 2$ eV) and exhibit enhanced photocatalytic efficiency due to their extra catalytic sites (Dom et al., 2011).

The ferrites formed on the graphene nanosheets can prevent agglomeration, while the graphene inhibits leaching of the toxic nanoparticles, enhancing both adsorption and photocatalytic performance by virtue of a large specific surface area, chemical stability, and lower electronic band gap. In addition, the GNSFs can be easily recovered using an external magnetic field after contaminant removal and reuse. According to the existing literature, the GNSFs are considered potential cost-effective alternatives to traditional adsorbents and photocatalysts. In this mini-review, we discuss recent progresses on the removal of recalcitrant environmental contaminants (particularly dyes, antibiotics, and heavy metal ions) using adsorption and photocatalysis. The studies using GNSFs as specific nano-adsorbents and photocatalysts are critically highlighted.

## 2. Synthesis technique of GNSFs

A literature search of the Web of Science database with both “graphene” and “ferrite” as keywords located 604 research articles published during the last decade, most of which (599) are reported in the last six years (Fig. 1). The largest fraction of papers on either adsorptive or photocatalytic removal of contaminants by GNSF came from China. Excluding self-citations, these papers were cited 1875 times (959 for adsorption and 916 for photocatalysis), and more than 1232 of them are dated from 2015 or later. These data show a clear growing trend of research and development of GNSFs as efficient adsorbents and/or photocatalysts. The most common ferrites used in the synthesis of GNSFs are cobalt ferrite ($CoFe_2O_4$) (18%) and bismuth ferrite (*i.e.,* perovskite ($BiFeO_3$), mullite ($Bi_2Fe_4O_9$), and sillenite ($Bi_{25}FeO_{40}$)) (17% together), possibly due to their high stability against corrosion and narrow bandgaps (0.8 and ~2.3 eV for cobalt (Shi et al., 2014) and bismuth ferrites, respectively (Hu et al., 2014, Yang et al., 2018a, Yang et al., 2018b) which enhance sunlight utilization.

Most of the GNSF nanohybrids comprising of cobalt/bismuth ferrite have been synthesized via a solvothermal/hydrothermal and co-precipitation pathway in solutions. Santhosh et al. (2017) synthesized $CoFe_2O_4$ by using solvothermal method first and then coated with silica ($SiO_2$) by sol-gel process. The obtained $SiO_2$@$CoFe_2O_4$ was functionalized with amino groups using 3-aminopropyltriethoxysilane and decorated on GO nanosheets at 80 °C for the adsorptive removal of organic and inorganic contaminants (*e.g.,* acid black I dye and Cr(VI) ions). Shi et al. (2014) prepared graphene-based $CoFe_2O_4$/CdS nanohybrid via a facile solvothermal method by adding 0.066 g of $Co(NO_3)_2{\cdot}6H_2O$ and 0.184 g of $Fe(NO_3)_3{\cdot}9H_2O$ to dispersed GO in absolute ethanol and autoclaving at 110 °C. Their obtained product was evaluated for its photocatalytic degradation performance for methylene blue (MB) dye under visible-light irradiation. Dat et al. (2018) synthesized the rGO/$CoFe_2O_4$ nanohybrid by using solvothermal method by dissolving 4 mmol of $FeCl_3{\cdot}6H_2O$ and 2 mmol of $Co(NO_3)_2{\cdot}6H_2O$ in a mixture of ethylene glycol and DI water and autoclaving at 190 °C. Then, the rGO/$CoFe_2O_4$/polyaniline (rGO/CF/PANI) was obtained by polymerization of aniline monomers

on the surface for use in uranium [(U(VI)] ion adsorption. Wu et al. (2015) synthesized rGO/$Bi_{25}FeO_{40}$ nanohybrid via a facile hydrothermal method by dissolving 2.426 g of $Bi(NO_3)_3{\cdot}5H_2O$ and 2.020 g of $Fe(NO_3)_3{\cdot}9H_2O$ in 60 mL of 1 M $HNO_3$ under stirring and autoclaving at 160 °C for 6 h for the photocatalytic degradation of phenol and *p*-chlorophenol under visible-light irradiation. Wang et al. (2017c) synthesized magnetic g-$C_3N_4$/$MnFe_2O_4$/graphene ($C_3N_4$@$MnFe_2O_4$-G) nanohybrid based on the solvothermal method using $MnCl_2{\cdot}4H_2O$ and $FeCl_3{\cdot}6H_2O$ as starting materials followed by impregnation approach. They have evaluated the photocatalytic activities for antibiotics (*e.g.*, metronidazole (MNZ), amoxicillin, tetracycline, and ciprofloxacin) degradation using persulfate (PS) under visible-light irradiation. Hu et al. (2015a) synthesized a 2D graphene-supported mullite bismuth ferrite ($BFO_{249}$/$rGO_{4.5}$) via a facile co-precipitation method by adding dispersed Bi/Fe into GO solution and heating at 95 °C for the adsorptive and photocatalytic degradation of BPA under solar irradiation. Several other synthesis routes have also been reported, including gamma-ray irradiation cross-linking technique for GO/chitosan/$CoFe_2O_4$ synthesis as a heterogeneous photo-Fenton catalyst (Al-Kahtani and Abou Taleb, 2016), ball-milling and heat treatment to prepare rGO/$CoFe_2O_4$ as a heterophotocatalyst (He et al., 2015), and multistep synthesis of Ag-decorated $Bi_2Fe_4O_9$ wrapped by rGO (BFO/Ag1/rGO) as a nanoscaled photocatalyst (Hu et al., 2015b).

A few reports selected zinc/manganese/nickel ferrites in the preparation of GNSFs due to a strong interest on their excellent magnetic and photocatalytic properties. Those GNSFs were synthesized using one-pot solvothermal/hydrothermal and co-precipitation routes. For example, Fei et al., 2016, Li et al., 2015, and Liu et al. (2017) successfully synthesized magnetic rGO/$ZnFe_2O_4$ via one-step solvothermal method by adding GO, $ZnCl_2$, and $FeCl_3{\cdot}6H_2O$ into ethylene glycol and autoclaving at 200 °C for the adsorption of MB, Cr(VI), and the selective degradation of ammonia, respectively. Kumar et al. (2014) and Huong et al. (2016) prepared GO/$MnFe_2O_4$ nanohybrids by co-precipitation technique by dissolving $FeCl_3{\cdot}6H_2O$ and $MnCl_2{\cdot}4H_2O$ in GO solution and heating at 80 °C for the adsorption of heavy metals (*i.e.*, Pb(II), As(III), and As(V)). Yamaguchi et al. (2016) combined rGO with $MnFe_2O_4$ via one-pot solvothermal process by dispersing $FeCl_3{\cdot}6H_2O$ and $MnCl_2{\cdot}4H_2O$ in ethylene glycol and autoclaving at 200 °C to inhibit the agglomeration of rGO for efficient glyphosate adsorption. Lingamdinne et al. (2016b) and Singh et al. (2017) fabricated GO/$NiFe_2O_4$ via one-step hydrothermal method by dissolving $Fe(NO_3)_3{\cdot}9H_2O$ and $Ni(NO_3)_3{\cdot}9H_2O$ in GO solution and heating at 80 °C for Pb(II)/Cr(III) removal and MB degradation under visible-light irradiation. Wang et al. (2017b) and Lingamdinne et al. (2017a) synthesized rGO/$NiFe_2O_4$ via one-pot hydrothermal/co-precipitation method by dispersing GO, $Fe(NO_3)_3{\cdot}9H_2O$, and $Ni(NO_3)_2{\cdot}6H_2O$ in aqueous solution and autoclaving at 220 °C to assess the adsorption properties for Congo Red (CR), methyl orange (MO), MB, Cr(VI), U(VI), Th(IV), As(III), and As(V). Liang et al. (2018) prepared rGO/$NiFe_2O_4$ via a simple mechanical ball-milling method to evaluate the photodegradation performance for MB under visible-light irradiation. In contrast, the copper/silver ferrites have not been widely used to prepare GNSF-based effective adsorbents and/or photocatalysts, despite the strong affinity of copper oxide to inorganic ions over a wide pH range and the relatively narrow band gap (1.9 eV) (Hosseini et al., 2017, Wu et al., 2018).

# 3. Major roles of GNSFs in water and wastewater treatment technologies

## 3.1. Adsorbent for contaminant removal

Adsorption is the most efficient approach in water and wastewater treatment technologies due to its low energy requirement, cost-effectiveness, and ease of application over a wide range of environmental conditions (Shafeeyan et al., 2010). Currently, GNSFs are recommended for the adsorptive removal of organic and inorganic contaminants, because these nanohybrids exhibit excellent adsorption capacity with their larger specific surface areas (*i.e.*, enhanced active binding sites) and larger effective pores. In addition, among other ferrites including garnet ($M_3Fe_5O_{12}$, M = rare earth cation), hexaferrite ($SrFe_{12}O_{19}$ and $BaFe_{12}O_{19}$), and orthoferrite ($MFeO_3$, M = rare earth cation) (Reddy and Yun, 2016), particular attention was given to spinel ferrites, mainly due to their simple chemical compositions and superparamagnetic properties. This section briefly discusses applications of GNSFs for the adsorption of organic and inorganic contaminants, and the corresponding adsorption capacities and mechanisms.

**3.1.1. Adsorption capacity of GNSFs—**The adsorption capacity of GNSFs as nano-adsorbents has been evaluated by adsorption isotherms (*e.g.*, Langmuir and Freundlich isotherms) and kinetic models (*e.g.*, pseudo-first and second order kinetics). Table 1 gives a concise summary of target organic and inorganic contaminants sorbed by GNSFs, the experimental conditions, the adsorption capacities, and the number of reuse cycles for the GNSFs. Compared to bare graphene-based nanomaterials (*e.g.*, graphene, GO, and rGO) or spinel ferrites, the GNSFs showed far better adsorption performance for the examined contaminants. For example, rGO/$Bi_2Fe_4O_9$ ($BFO_{249}$/$rGO_{4.5}$) (Hu et al., 2015a) exhibited a maximum adsorption capacity ($q_m$) of 3.95 mg $g^{-1}$ for BPA, which was more than two times higher than those of $BFO_{249}$ (0.74 mg $g^{-1}$) and GO/$Bi_2Fe_4O_9$ ($BFO_{249}$/$GO_{4.5}$) (1.72 mg $g^{-1}$) due to the increased surface area and formation of π-π stacking between the skeletal structure of rGO (specific surface area of ~2600 $m^2$ $g^{-1}$) and benzene ring in BPA (Perera et al., 2012). Kumar et al. (2014) reported that GO/$MnFe_2O_4$ (MFO-GO) also showed a high $q_m$ of 207 mg $g^{-1}$ for As(V) adsorption, which was much higher than the values of bare $MnFe_2O_4$ and GO nanosheets (136 and 113 mg $g^{-1}$, respectively).

For each GNSF, the types of cations at the tetrahedral/octahedral site and the contents of graphene are key parameters controlling the adsorption capacity (Wang et al., 2012). Increasing the GO content in MFO-GO from 10 to 50 wt% enhanced the adsorption performance for both MB and As(V) ions (Huong et al., 2016, Huong et al., 2018). The $q_m$ value of MFO-GO reached 177 and 240 mg $g^{-1}$ for MB and As(V) ions, respectively. In contrast, GO/$NiFe_2O_4$ (GONF) exhibited a much lower $q_m$ of 81.3 mg $g^{-1}$ for As(V), while that of rGO/$NiFe_2O_4$ (rGONF) was only slightly better (106 mg $g^{-1}$) (Lingamdinne et al., 2016a). The observed difference in $q_m$ is ascribed to the nature of cations deposited in GNSFs. Similarly, different $q_m$ values for Cr(VI) ions observed depending on different types of cations, being 501, 136, and 172 mg $g^{-1}$ for poly(m–phenylenediamine)/rGO/$NiFe_2O_4$ (PmPD/rGO/NFO) (Wang et al., 2017b), amino-functionalized $SiO_2$@$CoFe_2O_4$-GO (Santhosh et al., 2017), and 1,6–hexanediamine-functionalized rGO/$ZnFe_2O_4$ (HDA–rGO–$ZnFe_2O_4$) (Li et al., 2015), respectively.

Numerous studies have employed bare/polymer-grafted magnetic nanoparticles or similar graphene-based magnetic composites to remediate toxic heavy metals and organic dyes. However, their decontamination efficiencies were much lower than those of GNSFs. In the work of Asuha et al. (2011) and Zhou et al. (2013), the porous $Fe_3O_4$ nanopowder prepared by one-pot solvothermal reaction showed the $q_m$ of 15.4 and 6.2 mg $g^{-1}$ for Cr(VI) and MB dye. The magnetic $Fe_3O_4$@graphene composite (FGC) prepared by Yao et al. (2012) showed $q_m$ values of FGC reached 45.3 and 33.7 mg $g^{-1}$ for MB and CR dyes, respectively. Mishra and Ramaprabhu (2012) reported that the synthesized $Fe_3O_4$–graphene only achieved the $q_m$ of 172.1 and 180.3 mg $g^{-1}$ for As(III) and As(V) ions, respectively. The $Fe_3O_4$/GO composite prepared by Liu et al. (2011) exhibited low range $q_m$ of 13.0–22.7 mg $g^{-1}$ for Co(II).

**3.1.2. Adsorption mechanisms of GNSFs—**The key factors affecting the contaminant adsorption property are the types of adsorbate-GNSF interactions and the pH conditions (Fig. 2a). The most common physicochemical interactions responsible for the adsorption of contaminants include: electrostatic interactions, ion exchange, inner-sphere surface complexation, and **π-π** stacking (Reddy and Yun, 2016). Chemical adsorption (chemisorption) is attributed to the strong chemical binding when the GNSF shares electron pairs with the adsorbates, whereas physical adsorption (physisorption) results from weak attractive forces (*e.g.*, van der Waals, dipole-dipole interactions, hydrogen bonding, and *etc.*) between GNSFs and adsorbates (Sanghi and Verma, 2013). Adsorption studies of inorganic contaminants (*e.g.*, Cr(VI), U(VI), As(V), and Pb(II)) on various GNSFs have shown that the electrostatic interactions, ion exchange, and formation of the inner-sphere surface complexes are the dominant adsorption mechanisms, due to the protonation/deprotonation of surface functional groups of GNSFs over a wide range of pH. For example, the U(VI) ions were strongly bound to rGO/$CoFe_2O_4$/polyaniline (rGO/CF/PANI) through electrostatic interactions between the surface functional groups (S__$NH_2$, S═NH, and S__COOH, where S represents the surface) of the rGO/CF/PANI and U(VI) and hydrogen bonding (Dat et al., 2018). Using X-ray photoelectron spectroscopy (XPS), Fourier-transform infrared spectroscopy analysis, and 2-pKa diffusion layer modeling, Lingamdinne et al. (2017a) also reported on the formation of inner-sphere complexes between the oxygenated groups of rGO/$NiFe_2O_4$ (rGONF) (–C═O,__COO, and __C__O) and U(VI) or Th(IV). The As(V) ions were adsorbed on MFO-GO and rGONF by the combined effects of electrostatic interaction, ionic exchange process, and surface complexation due to the more abundant active sites including the oxygenated functional groups (*e.g.*, carboxyl (__OOH), epoxy (C__O), and hydroxyl (__OH) groups) (Huong et al., 2016, Huong et al., 2018, Lingamdinne et al., 2016a). XPS analysis also attributed As(III) and As(V) adsorptions on GO/$CuFe_2O_4$ supported on Fe__Ni foam (GCFF) to the ligand exchange of protonated surface hydroxyl groups of the GCFF by arsenate anions when the pH is below the point of zero charge (Wu et al., 2018).

The pH plays a significant role in the adsorption, because it determines the chemical speciation of the adsorbates as well as the surface charge of the GNSFs (Sun et al., 2015). Wang et al. (2017b) reported that the electrostatic interaction between negatively charged Cr(VI) species and the protonated PmPD/rGO/NFO played an important role in Cr(VI)

adsorption at pH = 3. Li et al. (2015) observed that HDA–rGO–$ZnFe_2O_4$ had better removal performances for Cr(VI) under acidic conditions, in which the protonated amine groups (__$NH_3^+$) of HDA would attract the negatively-charged Cr(VI) species electrostatically. In addition, the adsorbed Cr(VI) was reduced to Cr(III) and bound to the negatively-charged carboxylic groups of HDA–rGO–$ZnFe_2O_4$ through electrostatic interaction, which was confirmed by XPS analysis. Santhosh et al. (2017) reported that the negatively charged chromium species ($CrO_4^{2-}$, $HCrO_4^-$, and $Cr_2O_7^{2-}$) were attached to the protonated amino groups of the amino-functionalized $SiO_2$@$CoFe_2O_4$-GO by electrostatic interactions in acidic conditions (pH < 5). However, the adsorption capacity of GO/$MnFe_2O_4$ for Pb(II) ions was decreased at lower pH values, due to the formation of positively charged __$OH_2^+$ surface group, and/or increased competition of $H^+$ with metal ions for the active sites of adsorption (Kumar et al., 2014). In contrast, at higher pH, the adsorption performance of GO/$MnFe_2O_4$ was enhanced by the strong interaction between the deprotonated hydroxyl groups and Pb(II), and the cation exchange process with carboxylic functional groups.

The π-π stacking interaction was found to be the predominant adsorption mechanism for the removal of organic contaminants (*e.g.,* BPA and MB dye) on several GNSFs. Wang et al. (2017b) reported that the higher adsorption efficiency of rGO/$ZnFe_2O_4$ could be attributed to the π-π stacking interactions between rGO and MB molecules. Hu et al. (2015a) also showed that increasing the amount of rGO (wt%) in $BFO_{249}$/$GO_{4.5}$ enhanced the BPA adsorption due to the larger surface area and π-π stacking interactions between skeletal structures of rGO and hydrophobic BPA. Before that, in $BFO_{249}$/$GO_{4.5}$ the excessive functional groups of GO limited the π-π interaction and thereby lowered the BPA adsorption.

### 3.2 Photocatalyst for contaminant removal

Many recalcitrant organic contaminants can be photo-catalytically oxidized by reaction with highly reactive oxygen species (ROS) such as OH., $O_{2.}$-, and $HO_{2.}$ in the presence of nano-photocatalysts (Chong et al., 2010, Daghrir et al., 2013, Gaya and Abdullah, 2008). The organic intermediates formed during the oxidation process may also further react with those ROS, eventually leads to mineralization to innocuous gaseous molecules such as $CO_2$, $H_2O$, and $N_2$ (Casbeer et al., 2012, Chan et al., 2011, Zangeneh et al., 2015). Removal of organic contaminants from waters via the photocatalytic degradation routes is a major application area of GNSFs. The GNSFs can improve the photocatalytic degradation performance for organic contaminants while remaining chemically stable over a wide range of environmental conditions. Moreover, the presence of magnetic spinel ferrites in the GNSFs facilitates the separation process from the reaction system and enhances the reusability (Anjum et al., 2016). Since as much as 46% of the total energy in sunlight lies in the visible-light region (Casbeer et al., 2012, Rehman et al., 2009), GNSFs with narrower bandgaps (*e.g.,* 2.31 eV for $CoFe_2O_4$ (Dileep et al., 2014), 1.89 eV for $CuFe_2O_4$ (Köferstein et al., 2014), and 1.91 eV for $ZnFe_2O_4$ (Srivastava and Yadav, 2015)) would be more suitable than common semiconductors such as $TiO_2$ (3.2 eV) (Dette et al., 2014) and ZnO (3.2 eV) (Feng et al., 2014) in employing solar energy to photocatalytically degrade contaminants. Table 2 summarizes the target organic contaminants (*e.g.*, MB, MO, Rhodamine B (RhB), BPA, and 4-chlorophenol (4-CP)), experimental conditions, photocatalytic degradation performances,

and the number of reuses. Several GNSFs examined for photodegradation are discussed in the following sub-sections.

**3.2.1 Photocatalytic performance of GNSFs—**The adsorption process on GNSFs strongly affects the photocatalytic degradation of organic contaminants under visible-light irradiation (Fu et al., 2012). He et al. (2015) reported the photocatalytic degradation performance of rGO/$CoFe_2O_4$ reaching >93, 38, and 72% removal for MB, MO, and RhB dyes, respectively under visible-light irradiation. Their results demonstrated improved degradation of MB and RhB due to a higher adsorption capacity for cationic molecules, compared to the anionic MO. Liang et al. (2018) reported similar results, that rGO/$NiFe_2O_4$ exhibited superior photocatalytic performance for MB (99%) and RhB (82%) than for MO (47%) under visible-light illumination. Their result was attributed to the unfavorable adsorption of MO onto the negatively charged surface groups of rGO with electrostatic repulsion. Hu et al. (2015b) showed that the nanodesigned tribrid $Bi_2Fe_4O_9$/Ag (BFO/Ag1/rGO), with its larger surface area and higher density of active sites on rGO, promoted the mass transfer of dissolved MB molecules to increase the physical adsorption capacity (by up to 50%) in the dark condition. The rapid and enhanced degradation of MB occurred afterwards in the presence of $H_2O_2$ (20 mM) under visible-light irradiation. Hu et al. (2015a) reported that under visible-light irradiation, $BFO_{249}$/$rGO_{4.5}$ exhibited a synergistic adsorption-photocatalytic degradation effect (76 and 80% BPA removal at pH 6.5 and 5, respectively). Hosseini et al. (2017) also confirmed that the adsorption of organic molecules is a key factor for improved photocatalytic activity. They showed that approximately all the MB dye molecules were adsorbed on graphene/$AgFeO_2$ ($AgFeO_2$-G) due to the aromatic structure of the graphene-based system. As a result, most of the MB (>96%) were photocatalytically degraded within 40 min under visible-light illumination. Similar graphene-based non-magnetic photocatalysts such as ZnO-rGO (Nipane et al., 2015), $Mn_2O_3$-Graphene (Chandra et al., 2012), $Bi_2O_3$-rGO (Liu et al., 2013), BiOBr-GO (Vadivel et al., 2014), and $Ag_3PO_4$-GO (Chen et al., 2013) also exhibited high photodegradation efficiency against organic dyes (>84% for MB and >99% RhB). However, those materials require costly and inefficient separation of the photocatalysts.

**3.2.2 Photocatalytic degradation mechanisms of GNSFs—**The photocatalytic activity of the heterojunction nanohybrids is directly associated with the electronic band structures (*i.e.,* valence band (VB) and conduction band (CB)) of the constituent single-element nanoparticles, which determine the migration of photogenerated $e^-$ and the lifetime of the hole-$e^-$ (h-e) pairs. Fig. 2b schematically illustrates the excitation of GNSFs during the photocatalytic degradation process for organic contaminants under visible light. The noticeable increase in photocatalytic activity under visible-light illumination could be ascribed to OH and $O_2^-$ formation on the GNSFs through extensive movement of the photo-generated $e^-$ from VB to CB. For example, Wang et al. (2017c) showed that the photocatalytic activity against MNZ was noticeably improved by the heterojunction between graphene/$MnFe_2O_4$ with graphitic carbon nitride (g-$C_3N_4$) ($C_3N_4$@$MnFe_2O_4$-G) through an interfacial contact, leading to high transfer efficiency of photogenerated carriers and long lifetime of separated h-e pairs. Those authors performed radical trapping experiments with *p*-benzoquinone (*p*-BQ), methanol, dimethyl sulfoxide (DMSO), and ammonium oxalate

(AO) for $O_{2^{\cdot}}$, OH, photogenerated $e^-$, and $h^+$ quenchers, respectively. The photocatalytic degradation of MNZ in the $C_3N_4$@$MnFe_2O_4$-G/PS/vis system was suppressed in the order of AO > methanol > *p*-BQ > DMSO. This result confirmed that $O_{2^{\cdot -}}$, ·OH, and $h^+$ were the dominant species for the degradation of antibiotics under visible-light irradiation. Hosseini et al. (2017) reported that the higher photodegradation rate of RhB, MB, and MO dyes on $AgFeO_2$-G under visible-light irradiation can be attributed to the predominant OH species via decomposition of adsorbed $H_2O$. In addition, the photo-generated $e^-$ within $AgFeO_2$ can be transferred from the CB to rGO, which efficiently prevents the direct recombination of h-e pairs. Liang et al. (2018) showed that MB molecules adsorbed on rGO/$NiFe_2O_4$ by π−π stacking and electrostatic interaction were degraded by $h^+$, OH, and $O_{2}^{-}$. The dominant oxidative species in the photocatalytic degradation of MB was OH generated by reaction with $H_2O$ or $OH^-$ ion under visible-light irradiation. The $O_{2}^{-}$ was the minor species produced by the reaction of photogenerated $e^-$ with $O_2$. Shi et al. (2014) reported that the graphene-based–$CoFe_2O_4$/CdS (Gr–$CoFe_2O_4$/CdS) system had higher photocatalytic activity, which was derived from $CoFe_2O_4$ due to the lower electronic band gap (0.8 eV). The photo-excited $e^-$ in $CoFe_2O_4$ migrated to the CB of CdS through the graphene as an electron mediator. During this process, OH and $O_{2^{\cdot -}}$ are formed, acting as the main species for MB dye degradation.

GNSFs exhibit a higher degree of light harvesting properties with broader absorption in the visible-light region, which could be attributed to the presence of graphene (Moussa et al., 2016). The increased amount of graphene also enhances the light absorption in the visible region. Therefore, the visible-light harvesting capability can be tailored by controlling the content of graphene, and visible-light can be better utilized by the optimized GNSF catalysts for photocatalytic degradation of organic molecules. In addition, the graphene in GNSFs plays the roles of photogenerated $e^-$ acceptor and mediator, so that the recombination of h-e pairs can be inhibited in the transfer process. Liu et al. (2017) showed that the transfer of photogenerated $e^-$ on the CB of $ZnFe_2O_4$ to rGO was energetically favorable under visible-light irradiation. The rGO acted as a “sink” for the photogenerated $e^-$ (storing electrons in its huge π–π network) due to the lower Fermi energy of rGO compared to the CB of $ZnFe_2O_4$. As such, rGO inhibited the h-e recombination on $ZnFe_2O_4$ and facilitated the interface charge separation. Singh et al. (2017) also reported that nitrogen-doped graphene/$NiFe_2O_4$ ($NiFe_2O_4$-NG) not only enhanced the adsorption of MB dye by π-π interactions with the aromatic rings of hydrophobic MB molecules, but also restricted direct h-e recombination by trapping the delocalized electrons. Hu et al. (2015a) showed that the higher photocatalytic degradation efficiency of $BFO_{249}$/$rGO_{4.5}$ for BPA was due to the synergistic effect between adsorption and photocatalytic degradation, including enhanced adsorption of BPA by π–π stacking interactions and ROS generation. The photoexcited $e^-$ in $BFO_{249}$ could migrate through the extended π-conjugated aromatic region of rGO and then become trapped by the adsorbed $O_2$ to form $O_{2}^{-}$, while the recombination of photogenerated h-e pairs was retarded by rGO.

Fe ions in GNSFs could enhance the ROS generation under visible-light irradiation through the Fenton-like reaction (*i.e.*, photo-Fenton process), which contributes to the catalytic oxidation of target organic compounds and thus overcomes drawbacks of traditional Fenton processes (*e.g.*, narrower working pH, higher iron waste, and higher demand of $H_2O_2$

(Pariente et al., 2008)). Hu et al. (2015b) investigated the heterogeneous photo-Fenton process under visible-light illumination. They concluded that in the BFO/Ag1/rGO/$H_2O_2$ system, Fe(II) is converted to Fe(III) under visible-light irradiation, while the photogenerated $e^-$ can be easily transferred from BFO to Ag nanoparticles through the heterojunction and rGO, simultaneously consuming $H_2O_2$ and forming ROS (*e.g.*, OH and $O_2^-$) on the surface of BFO/Ag1/rGO (Eqs. (1), (2)).

$$H_2O_2 + e^- + H^+ \rightarrow OH^\bullet + H_2O \quad (1)$$

$$O_2 + e^- \rightarrow O_2^{\bullet -} \quad (2)$$

The OH species are further produced through the reduction of Fe(III) to Fe(II) under visible-light illumination (Eq. (3)). rGO also played an important role in inhibiting the recombination of h-e pairs.

$$\mathrm{BFO\,(Fe(III))} + 2H_2O_2 + h\upsilon(\lambda > 420\,\mathrm{nm}) \rightarrow \mathrm{BFO\,(Fe(II))} + OH^\bullet + H_2O + O_2 + H^+ \quad (3)$$

Al-Kahtani and Abou Taleb (2016) showed that the significantly enhanced photo-Fenton activity in chitosan/GO/$CoFe_2O_4$ could be ascribed to the effective separation of the h-e pairs, which generated not only OH by reaction of trapped $OH^-$ or $H_2O_2$ with the photogenerated $h^+$ and $e^-$ on the CF, but also $O_2$by reaction of $O_2$ with $e^-$ migrated from the CF on GO.

$$CoFe_2O_4 + h\upsilon \rightarrow CoFe_2O_4\,(h^+ + e^-) \quad (4)$$

$$CoFe_2O_4\,(e^-) + \mathrm{graphene} \rightarrow CoFe_2O_4 + \mathrm{graphene}\,(e^-) \quad (5)$$

$$CoFe_2O_4\,(e^-) + H_2O_2 \rightarrow CoFe_2O_4 + OH^- + \bullet OH \quad (6)$$

$$\mathrm{Graphene}\,(e^-) + O_2 \rightarrow O_2^{\bullet -} + \mathrm{graphene} \quad (7)$$

$$CoFe_2O_4\,(h^+) + OH^- \rightarrow CoFe_2O_4 + \bullet OH \quad (8)$$

## 4. Magnetic recovery and reuse of GNSFs

The reuse potential of new nanohybrid materials is crucial for upscaling commercial applications. After removing organic and inorganic contaminants from aqueous solutions, an external magnetic field can penetrate glass/plastic materials to separate the used GNSFs

without filtration. Such magnetic separation is not very sensitive to the working conditions such as the pH, temperature, and ionic strength (Pamme, 2006). Then, the GNSFs can be regenerated by several desorption processes. Wu et al. (2018) utilized ultrasonication for the regeneration of the arsenic-contained adsorbent with NaOH solution. For metal-loaded adsorbents, the HCl and $HNO_3$ solutions have also been used as a desorbing agent for regeneration (Chella et al., 2015, Kumar et al., 2014, Lingamdinne et al., 2016b). Wang et al. (2017c) only washed the spent photocatalyst with DI water and ethanol followed by drying at 60 °C. A high degree of desorption can be achieved under alkaline conditions for the recycling of adsorbents loaded with anionic pollutants (Gupta et al., 2007, Santhosh et al., 2017). These promising points indicate that the GNSFs are cost-effective adsorbents and photocatalysts that could be recycled. Moreover, the GNSFs can prevent nanoparticle release into natural waters, which may have unknown environmental effects.

Among the reviewed studies, $AgFeO_2$-G developed by Hosseini et al. (2017) was successfully reused in the degradation of MB for 10 cycles without significant loss of photocatalytic activity. Other works have also shown that the various GNSFs can be continuously recycled with no considerable reduction in photocatalytic activity, as presented in Table 1, Table 2. For example, Santhosh et al. (2017) reported that acid black I dye and Cr(VI) ions adsorbed on the amino-functionalized $SiO_2$@$CoFe_2O_4$-GO nanohybrids could be desorbed in an agent (0.1 M NaOH) for regeneration. Through five cycles of adsorption-desorption processes, the nanohybrid adsorbents showed high reusability potential. In the study by Wu et al. (2018), the adsorptive arsenic removal efficiency by GCFF only started to deteriorate after the 9th regeneration cycle during a 10-cycle adsorption–desorption test. Wang et al. (2017c) showed that the photocatalytic activity of regenerated $C_3N_4$@$MnFe_2O_4$-G was not significantly reduced after five recycles, indicating that the photocatalyst had great stability in repeated use in antibiotic degradation. The reduced adsorption/photocatalytic degradation performance after a critical number of recycles can be attributed to incomplete desorption of adsorbates and/or adsorbent loss during the regeneration processes (Joo et al., 2013). On the other hand, during several regeneration cycles, the GNSFs may have changed physicochemical properties or undergo irreversible particle-particle aggregation, reducing the efficacy of contaminant removal (Hankare et al., 2011, Xia et al., 2011). The schematic diagram of GNSFs reuse process in aqueous solution is illustrated in Fig. 3.

## 5. Conclusions

This review summarizes recent progresses of novel GNSFs with a focus on their application in water remediation. As illustrated, the graphene-based cobalt/bismuth ferrite has been synthesized by numerous methods including solvothermal/hydrothermal and co-precipitation for use as highly effective adsorbents and photocatalysts. In most cases, GNSFs are preferred adsorbents for the removal of organic and inorganic contaminants from aqueous solutions, due to their excellent adsorption capacity compared to single-element graphene/GO/rGO or spinel ferrites. Correspondingly, these novel GNSFs have shown great photocatalytic performance under visible-light irradiation. Furthermore, the reusability potential of the GNSFs following non-invasive separation is discussed, showing the advantages and limitations in recycling GNSFs. In conclusion, there are growing demands

for magnetically separable/recyclable adsorbents and solar-driven photocatalysts in environmental remediation. In this regard, the use of GNSFs is quite promising in the oxidative degradation of recalcitrant organic contaminants or reduction of inorganic contaminants using GNSFs in photocatalytic systems. However, the tendency for self-agglomeration and toxicity concerns raised by the metallic nanoparticles release are major hurdles in the field- and full-scale applications of GNSFs to real-life water remediation. The surface modification (*i.e.,* coating of GNSFs with naturally occurring and synthetic organic materials) can be a promising solution in reducing their toxicity, inhibiting agglomeration, and increasing adsorptive and photocatalytic activities. We hope this review will guide future research to fully utilize GNSFs in the water remediation technology.

## Acknowledgments

This study was supported by the Basic Science Research Program through the National Research Foundation of Korea (NRF) funded by the Ministry of Education (NRF-2018R1A6A1A03024962 and NRF-2018R1D1A1B07040341), and the Korea Ministry of Environment (The SEM projects; 2018002470005). This publication does not reflect United States Environmental Protection Agency's policy. The research presented was not performed or funded by EPA and was not subject to EPA's quality system requirements. The views expressed in this article are those of the authors and do not necessarily represent the views or policies of the U.S. Environmental Protection Agency.

## Abbreviations

| | |
|---|---|
| **AO** | Ammonium oxalate |
| **BFO** | $Bi_2Fe_4O_9$ |
| **BPA** | Bisphenol A |
| **CB** | Conduction band |
| **CF** | $CoFe_2O_4$ |
| **4-CP** | 4-Chlorophenol |
| **CR** | Congo Red |
| **DMSO** | Dimethyl sulfoxide |
| **G** | Graphene |
| **GCFF** | GO/$CuFe_2O_4$ supported on Fe__Ni foam |
| **GNFSs** | Graphene-based nano spinel ferrites |
| **GO** | Graphene oxide |
| **GONF** | GO/$NiFe_2O_4$ |
| **HAD** | 1,6–Hexanediamine |
| **MB** | Methylene blue |
| **MFO** | $MnFe_2O_4$ |

| | |
|---|---|
| **MNZ** | Metronidazole |
| **MO** | Methyl orange |
| **NF** | $NiFe_2O_4$ |
| **NFO** | $NiFe_2O_4$ |
| **PANI** | Polyaniline |
| ***p*-BQ** | *p*-Benzoquinone |
| **PS** | Persulfate |
| **PmPD** | m–Phenylenediamine |
| **rGO** | Reduced graphene oxide |
| **rGONF** | $rGO/NiFe_2O_4$ |
| **RhB** | Rhodamine B |
| **ROS** | Reactive oxygen species |
| **VB** | Valence band |
| **XPS** | X-ray photoelectron spectroscopy |

## References


Al-Hamadani YA, Lee G, Kim S, Park CM, Jang M, Her N, Han J, Kim D-H, Yoon Y Sonocatalytic degradation of carbamazepine and diclofenac in the presence of graphene oxides in aqueous solution Chemosphere, 205 (2018), pp. 719–727 [PubMed: 29730472]

Al-Kahtani AA, Abou MF Taleb Photocatalytic degradation of MaxiIon CI basic dye using CS/$CoFe_2O_4$/GONCs as a heterogeneous photo-Fenton catalyst prepared by gamma irradiation J. Hazard Mater, 309 (2016), pp. 10–19 [PubMed: 26872328]

Anjum M, Miandad R, Waqas M, Gehany F, Barakat M Remediation of wastewater using various nano-materials Arab. J. Chem (2016)

Archer E, Petrie B, Kasprzyk-Hordern B, Wolfaardt GM The fate of pharmaceuticals and personal care products (PPCPs), endocrine disrupting contaminants (EDCs), metabolites and illicit drugs in a WWTW and environmental waters Chemosphere, 174 (2017), pp. 437–446 [PubMed: 28187390]

Asuha S, Suyala B, Zhao S Porous structure and Cr(VI) removal abilities of Fe3O4 prepared from Fe–urea complex Mater. Chem. Phys, 129 (1–2) (2011), pp. 483–487

Bao L Shen Y Wang P Padhan A Gupta A facile thermolysis route to monodisperse ferrite nanocrystals J. Am. Chem. Soc, 129 (41) (2007), pp. 12374–12375 [PubMed: 17880220]

Casbeer E, Sharma VK, Li X-Z Synthesis and photocatalytic activity of ferrites under visible light: a review Separ. Purif. Technol, 87 (2012), pp. 1–14

Chan SHS, Yeong Wu T, Juan JC, The CY Recent developments of metal oxide semiconductors as photocatalysts in advanced oxidation processes (AOPs) for treatment of dye waste-water J. Chem. Technol. Biotechnol, 86 (9) (2011), pp. 1130–1158

Chandra P Das S Bag R Bhar P Pramanik Mn2O3 decorated graphene nanosheet: an advanced material for the photocatalytic degradation of organic dyes Mater. Sci. Eng., B, 177 (11) (2012), pp. 855–861

Chella S, Kollu P, Komarala E, Doshi S, Saranya M, Felix S, Ramachandran R, Saravanan P, Koneru VL, Venugopal V, Jeong SK, Grace AN Solvothermal synthesis of $MnFe_2O_4$-graphene composite-Investigation of its adsorption and antimicrobial properties Appl. Surf. Sci, 327 (2015), pp. 27–36

Chen G, Sun M, Wei Q, Zhang Y, Zhu B, Du B $Ag_3PO_4$/graphene-oxide composite with remarkably enhanced visible-light-driven photocatalytic activity toward dyes in water J. Hazard Mater, 244 (2013), pp. 86–93 [PubMed: 23246944]

Chong MN, Jin B, Chow CW, Saint C Recent developments in photocatalytic water treatment technology: a review Water Res., 44 (10) (2010), pp. 2997–3027 [PubMed: 20378145]

Daghrir R, Drogui P, Robert Modified D $TiO_2$ for environmental photocatalytic applications: a review Ind. Eng. Chem. Res, 52 (10) (2013), pp. 3581–3599

Dat TQ, Ha NT, Van Thin P, Tung NV, Hung DQ Synthesis of RGO/CF/PANI magnetic composites for effective adsorption of uranium IEEE Trans. Magn, 54 (6) (2018)

Deng X, Lü L, Li H, Luo F The adsorption properties of Pb(II) and Cd(II) on functionalized graphene prepared by electrolysis method J. Hazard Mater, 183 (1–3) (2010), pp. 923–930 [PubMed: 20800353]

Dette C, Pérez-Osorio MA, Kley CS, Punke P, Patrick CE, Jacobson P, Giustino F, Jung SJ, Kern K $TiO_2$ anatase with a bandgap in the visible region Nano Lett., 14 (11) (2014), pp. 6533–6538 [PubMed: 25252265]

Devi LG, Srinivas M Hydrothermal synthesis of reduced graphene oxide-$CoFe_2O_4$ heteroarchitecture for high visible light photocatalytic activity: exploration of efficiency, stability and mechanistic pathways J. Environ. Chem. Eng, 5 (4) (2017), pp. 3243–3255

Dileep K, Loukya B, Pachauri N, Gupta A, Datta R Probing optical band gaps at the nanoscale in $NiFe_2O_4$ and $CoFe_2O_4$ epitaxial films by high resolution electron energy loss spectroscopy J. Appl. Phys, 116 (10) (2014), p. 103505

Dom R, Subasri R, Radha K, Borse PH Synthesis of solar active nanocrystalline ferrite, MFe2O4 (M: Ca, Zn, Mg) photocatalyst by microwave irradiation Solid State Commun., 151 (6) (2011), pp. 470–473

Fei P, Qiao J, Huo JX, Liu JH, Zhong M, Su Barium BT (II)-doped zinc ferrite. reduced graphene oxide nanohybrids for superior adsorption and magnetic properties N. Carbon Mater, 32 (5) (2017), pp. 402–410

Fei P, Wang Q, Zhong M, Su Preparation BT and adsorption properties of enhanced magnetic zinc ferrite-reduced graphene oxide nanocomposites via a facile one-pot solvothermal method J. Alloy. Comp, 685 (2016), pp. 411–417

Feng X, Guo H, Patel K, Zhou H, Lou High performance X, recoverable $Fe_3O_4$ZnO nanoparticles for enhanced photocatalytic degradation of phenol Chem. Eng. J, 244 (2014), pp. 327–334

Fu Y, Chen H, Sun X, Wang X Combination of cobalt ferrite and graphene: high-performance and recyclable visible-light photocatalysis Appl. Catal., B, 111 (2012), pp. 280–287

Gaya UI, Abdullah AH Heterogeneous photocatalytic degradation of organic contaminants over titanium dioxide: a review of fundamentals, progress and problems J. Photochem. Photobiol., C, 9 (1) (2008), pp. 1–12

Ghobadi M, Gharabaghi M, Abdollahi H, Boroumand Z, Moradian M $MnFe_2O_4$-graphene oxide magnetic nanoparticles as a high-performance adsorbent for rare earth elements: synthesis, isotherms, kinetics, thermodynamics and desorption J. Hazard Mater, 351 (2018), pp. 308–316 [PubMed: 29554528]

Ghosh BK, Moitra D, Chandel M, Ghosh Preparation of NN $TiO_2$/cobalt ferrite/reduced graphene oxide nanocomposite based magnetically separable catalyst with improved photocatalytic activity J. Nanosci. Nanotechnol, 17 (7) (2017), pp. 4694–4703

Goodwin DG Jr., Adeleye AS, Sung L, Ho KT, Burgess RM, Petersen EJ Detection and quantification of graphene-family nanomaterials in the environment Environ. Sci. Technol, 52 (8) (2018), pp. 4491–4513

Gupta VK, Ali I, Saini VK Defluoridation of wastewaters using waste carbon slurry Water Res., 41 (15) (2007), pp. 3307–3316 [PubMed: 17583767]

Hankare P, Patil R, Jadhav A, Garadkar K, Sasikala R Enhanced photocatalytic degradation of methyl red and thymol blue using titania–alumina–zinc ferrite nanocomposite Appl. Catal., B, 107 (3–4) (2011), pp. 333–339

He GY, Ding JJ, Zhang JG, Hao QL, Chen HQ One-step ball-milling preparation of highly photocatalytic active $CoFe_2O_4$-reduced graphene oxide heterojunctions for organic dye removal Ind. Eng. Chem. Res, 54 (11) (2015), pp. 2862–2867

Hosseini SM, Hosseini-Monfared H, Abbasi V Silver ferrite-graphene nanocomposite and its good photocatalytic performance in air and visible light for organic dye removal Appl. Organomet. Chem, 31 (4) (2017)

Hu Z-T, Chen B, Lim Single-crystalline T-T Bi2Fe4O9 synthesized by low-temperature co-precipitation: performance as photo-and Fenton catalysts RSC Adv., 4 (53) (2014), pp. 27820–27829

Hu ZT, Liu JC, Yan XL, Oh WD, Lim TT Low-temperature synthesis of graphene/$Bi_2Fe_4O_9$ composite for synergistic adsorption-photocatalytic degradation of hydrophobic pollutant under solar irradiation Chem. Eng. J, 262 (2015a), pp. 1022–1032

Hu ZT, Lua SK, Lim Cuboid-like TT $Bi_2Fe_4O_9$/Ag with graphene-wrapping tribrid composite with superior capability for environmental decontamination: nanoscaled material design and visible-light-driven multifunctional catalyst ACS Sustain. Chem. Eng, 3 (11) (2015b), pp. 2726–2736

Huong PTL, Huy LT, Phan VN, Huy TQ, Nam MH, Lam VD, Le AT Application of graphene oxide-$MnFe_2O_4$ magnetic nanohybrids as magnetically separable adsorbent for highly efficient removal of arsenic from water J. Electron. Mater, 45 (5) (2016), pp. 2372–2380

Huong PTL, Tu N, Lan H, Thang LH, Quy NV, Tuan PA, Dinh NX, Phan VN, Le AT Functional manganese ferrite/graphene oxide nanocomposites: effects of graphene oxide on the adsorption mechanisms of organic MB dye and inorganic As(V) ions from aqueous solution RSC Adv., 8 (22) (2018), pp. 12376–12389

Inyang M, Gao B, Zimmerman A, Zhang M, Chen H Synthesis, characterization, and dye sorption ability of carbon nanotube–biochar nanocomposites Chem. Eng. J, 236 (2014), pp. 39–46

Jin Q, Zhang S, Wen T, Wang J, Gu P, Zhao G, Wang X, Chen Z, Hayat T, Wang X Simultaneous adsorption and oxidative degradation of Bisphenol A by zero-valent iron/iron carbide nanoparticles encapsulated in N-doped carbon matrix Environ. Pollut, 243 (2018), pp. 218–227 [PubMed: 30176495]

Joo J, Ye Y, Kim D, Lee J, Jeon S Magnetically recoverable hybrid $TiO_2$ nanocrystal clusters with enhanced photocatalytic activity Mater. Lett, 93 (2013), pp. 141–144

Köferstein R, Walther T, Hesse D, Ebbinghaus Crystallite-growth SG, phase transition, magnetic properties, and sintering behaviour of nano-$CuFe_2O_4$ powders prepared by a combustion-like process J. Solid State Chem, 213 (2014), pp. 57–64

Kumar S, Nair RR, Pillai PB, Gupta SN, Iyengar MAR, Sood AK Graphene oxide-MnFe2O4 magnetic nanohybrids for efficient removal of lead and arsenic from water ACS Appl. Mater. Interfaces, 6 (20) (2014), pp. 17426–17436 [PubMed: 25222124]

Li HZ, Zhang L, Sun ZB, Liu Y, Yang B, Yan SQ One-step synthesis of magnetic 1,6-hexanediamine-functionalized reduced graphene oxide-zinc ferrite for fast adsorption of Cr(VI) RSC Adv., 5 (40) (2015), pp. 31787–31797

Liang JX, Wei Y, Zhang JG, Yao Y, He GY, Tang B, Chen HQ Scalable green method to fabricate magnetically separable $NiFe_2O_4$-reduced graphene oxide nanocomposites with enhanced photocatalytic performance driven by visible light Ind. Eng. Chem. Res, 57 (12) (2018), pp. 4311–4319

Lingamdinne LP, Choi YL, Kim IS, Chang YY, Koduru JR, Yang JK Porous graphene oxide based inverse spinel nickel ferrite nanocomposites for the enhanced adsorption removal of arsenic RSC Adv., 6 (77) (2016a), pp. 73776–73789

Lingamdinne LP, Choi YL, Kim IS, Yang JK, Koduru JR, Chang YY Preparation and characterization of porous reduced graphene oxide based inverse spinel nickel ferrite nanocomposite for adsorption removal of radionuclides J. Hazard Mater, 326 (2017a), pp. 145–156 [PubMed: 28013158]

Lingamdinne LP, Kim IS, Ha JH, Chang YY, Koduru JR, Yang JK Enhanced adsorption removal of Pb(II) and Cr(III) by using nickel ferrite-reduced graphene oxide nanocomposite Metals, 7 (6) (2017b)

Lingamdinne LP, Koduru JR, Choi YL, Chang YY, Yang JK Studies on removal of Pb(II) and Cr(III) using graphene oxide based inverse spinel nickel ferrite nano-composite as sorbent Hydrometallurgy, 165 (2016b), pp. 64–72

Liu M, Chen C, Hu J, Wu X, Wang X Synthesis of magnetite/graphene oxide composite and application for cobalt (II) removal J. Phys. Chem. C, 115 (51) (2011), pp. 25234–25240

Liu SQ, Zhu XL, Zhou Y, Meng ZD, Chen ZG, Liu CB, Chen F, Wu ZY, Qian JC Smart photocatalytic removal of ammonia through molecular recognition of zinc ferrite/reduced graphene oxide hybrid catalyst under visible-light irradiation Catal. Sci. Technol, 7 (15) (2017), pp. 3210–3219

Liu X, Pan L, Lv T, Sun Z, Sun CQ Visible light photocatalytic degradation of dyes by bismuth oxide-reduced graphene oxide composites prepared via microwave-assisted method J. Colloid Interface Sci, 408 (2013), pp. 145–150 [PubMed: 23953652]

Mishra A, Ramaprabhu S Ultrahigh arsenic sorption using iron oxide-graphene nanocomposite supercapacitor assembly J. Appl. Phys, 112 (10) (2012), p. 104315

Moitra D, Chandel M, Ghosh BK, Jani RK, Patra MK, Vadera SR, Ghosh NN A simple 'in situ' co-precipitation method for the preparation of multifunctional CoFe2O4-reduced graphene oxide nanocomposites: excellent microwave absorber and highly efficient magnetically separable recyclable photocatalyst for dye degradation RSC Adv., 6 (80) (2016)

Moussa H, Girot E, Mozet K, Alem H, Medjahdi G, Schneider R ZnO rods reduced graphene oxide composites prepared via a solvothermal reaction for efficient sunlight-driven photocatalysis Appl. Catal., B, 185 (2016), pp. 11–21

Naskar A, Khan H, Jana S One pot low temperature synthesis of graphene coupled Gd-doped ZnFe2O4 nanocomposite for effective removal of antibiotic levofloxacin drug J. Sol. Gel Sci. Technol, 86 (3) (2018), pp. 599–609

Nipane S, Korake P, Gokavi G Graphene-zinc oxide nanorod nanocomposite as photocatalyst for enhanced degradation of dyes under UV light irradiation Ceram. Int, 41 (3) (2015), pp. 4549–4557

Pamme N Magnetism and microfluidics Lab Chip, 6 (1) (2006), pp. 24–38 [PubMed: 16372066]

Pariente MI, Martinez F, Melero JA, Botas JA, Velegraki T, Xekoukoulotakis NP, Mantzavinos D Heterogeneous photo-Fenton oxidation of benzoic acid in water: effect of operating conditions, reaction by-products and coupling with biological treatment Appl. Catal., B, 85 (1–2) (2008), pp. 24–32

Park CM, Heo J, Wang D, Su C, Yoon Y Heterogeneous activation of persulfate by reduced graphene oxide–elemental silver/magnetite nanohybrids for the oxidative degradation of pharmaceuticals and endocrine disrupting compounds in water Appl. Catal., B, 225 (2018), pp. 91–99

Park CM, Heo J, Yoon Y Oxidative degradation of bisphenol A and 17α-ethinyl estradiol by Fenton-like activity of silver nanoparticles in aqueous solution Chemosphere, 168 (2017), pp. 617–622 [PubMed: 27838031]

Peng XY, Qu JY, Tian S, Ding YW, Hai X, Jiang B, Wu MB, Qiu JS Green fabrication of magnetic recoverable graphene/MnFe2O4 hybrids for efficient decomposition of methylene blue and the Mn/Fe redox synergetic mechanism RSC Adv., 6 (106) (2016), pp. 104549–104555

Perera SD, Mariano RG, Vu K, Nour N, Seitz O, Chabal Y, Balkus KJ Jr. Hydrothermal synthesis of graphene-TiO2 nanotube composites with enhanced photocatalytic activity ACS Catal., 2 (6) (2012), pp. 949–956

Rani GJ, Rajan MAJ, Kumar GG Reduced graphene oxide/$ZnFe_2O_4$ nanocomposite as an efficient catalyst for the photocatalytic degradation of methylene blue dye Res. Chem. Intermed, 43 (4) (2017), pp. 2669–2690

Reddy DHK, Yun Y-S Spinel ferrite magnetic adsorbents: alternative future materials for water purification? Coord. Chem. Rev, 315 (2016), pp. 90–111

Rehman S, Ullah R, Butt A, Gohar N Strategies of making $TiO_2$ and ZnO visible light active J. Hazard Mater, 170 (2–3) (2009), pp. 560–569 [PubMed: 19540666]

Sanghi R, Verma P Decolorisation of aqueous dye solutions by low-cost adsorbents: a review Color. Technol., 129 (2) (2013), pp. 85–108

Santhosh C, Daneshvar E, Kollu P, Peraniemi S, Grace AN, Bhatnagar Magnetic A $SiO_2$@$CoFe_2O_4$ nanoparticles decorated on graphene oxide as efficient adsorbents for the removal of anionic pollutants from water Chem. Eng. J, 322 (2017), pp. 472–487

Santhosh C, Kollu P, Felix S, Velmurugan V, Jeong SK, Grace AN CoFe2O4 and NiFe2O4@graphene adsorbents for heavy metal ions - kinetic and thermodynamic analysis RSC Adv., 5 (37) (2015), pp. 28965–28972

Shafeeyan MS, Daud WMAW, Houshmand A, Shamiri A A review on surface modification of activated carbon for carbon dioxide adsorption J. Anal. Appl. Pyrolysis, 89 (2) (2010), pp. 143–151

Shi YQ, Zhou KQ, Wang BB, Jiang SH, Qian XD, Gui Z, Yuen RKK, Hu Y Ternary graphene-CoFe2O4/CdS nanohybrids: preparation and application as recyclable photocatalysts J. Mater. Chem. A, 2 (2) (2014), pp. 535–544

Singh R, Ladol J, Khajuria H, Sheikh HN Nitrogen doped graphene nickel ferrite magnetic photocatalyst for the visible light degradation of methylene blue Acta Chim. Sin, 64 (1) (2017), pp. 170–178

Srivastava R, Yadav B Nanostructured ZnFe2O4 thick film as room temperature liquefied petroleum gas sensor J. Exp. Nanosci, 10 (9) (2015), pp. 703–717

Sun W, Pan W, Wang F, Xu N Removal of Se(IV) and Se(VI) by MFe2O4 nanoparticles from aqueous solution Chem. Eng. J, 273 (2015), pp. 353–362

Tan L, Liu Q, Song D, Jing X, Liu J, Li R, Hu S, Liu L, Wang J Uranium extraction using a magnetic $CoFe_2O_4$–graphene nanocomposite: kinetics and thermodynamics studies New J. Chem, 39 (4) (2015), pp. 2832–2838

Tran DQ, Pham HT, Do HQ Efficient removal of uranium from aqueous solution by reduced graphene oxide-$Zn_{0.5}Ni_{0.5}Fe_2O_4$ ferrite-polyaniline nanocomposite J. Electron. Mater, 46 (6) (2017), pp. 3273–3278

Vadivel S, Vanitha M, Muthukrishnaraj A, Balasubramanian N Graphene oxide–BiOBr composite material as highly efficient photocatalyst for degradation of methylene blue and rhodamine-B dyes J. Water Process Eng, 1 (2014), pp. 17–26

Veldhoen N, Skirrow RC, Brown LL, van Aggelen G, Helbing CC Effects of acute exposure to the non-steroidal anti-inflammatory drug ibuprofen on the developing North American bullfrog (Rana catesbeiana) tadpole Environ. Sci. Technol, 48 (17) (2014), pp. 10439–10447 [PubMed: 25111458]

Wang D, Park CM, Masud A, Aich N, Su C Carboxymethylcellulose mediates the transport of carbon nanotube-magnetite nanohybrid aggregates in water-saturated porous media Environ. Sci. Technol, 51 (21) (2017a), pp. 12405–12415 [PubMed: 29037033]

Wang L, Li J, Wang Y, Zhao L, Jiang Q Adsorption capability for Congo red on nanocrystalline MFe2O4 (M= Mn, Fe, Co, Ni) spinel ferrites Chem. Eng. J, 181 (2012), pp. 72–79

Wang W, Cai K, Wu XF, Shao XH, Yang XJ A novel poly(m-phenylenediamine)/reduced graphene oxide/nickel ferrite magnetic adsorbent with excellent removal ability of dyes and Cr(VI) J. Alloy. Comp, 722 (2017b), pp. 532–543

Wang XY, Wang AQ, Ma J Visible-light-driven photocatalytic removal of antibiotics by newly designed $C_3N_4$@$MnFe_2O_4$-graphene nanocomposites J. Hazard Mater, 336 (2017c), pp. 81–92 [PubMed: 28475915]

Wu LK, Wu H, Zhang HB, Cao HZ, Hou GY, Tang YP, Zheng Graphene oxide GQ/$CuFe_2O_4$ foam as an efficient absorbent for arsenic removal from water Chem. Eng. J, 334 (2018), pp. 1808–1819

Wu Y, Luo HJ, Jiang XL, Wang H, Geng JJ Facile synthesis of magnetic Bi25FeO40/rGO catalyst with efficient photocatalytic performance for phenolic compounds under visible light RSC Adv., 5 (7) (2015), pp. 4905–4908

Xia J, Wang A, Liu X, Su Z Preparation and characterization of bifunctional, Fe3O4/ZnO nanocomposites and their use as photocatalysts Appl. Surf. Sci, 257 (23) (2011), pp. 9724–9732

Xiong W, Zeng G, Yang Z, Zhou Y, Zhang C, Cheng M, Liu Y, Hu L, Wan J, Zhou C Adsorption of tetracycline antibiotics from aqueous solutions on nanocomposite multi-walled carbon nanotube functionalized MIL-53 (Fe) as new adsorbent Sci. Total Environ, 627 (2018), pp. 235–244 [PubMed: 29426146]

Yamaguchi NU, Bergamasco R, Hamoudi Magnetic S $MnFe_2O_4$-graphene hybrid composite for efficient removal of glyphosate from water Chem. Eng. J, 295 (2016), pp. 391–402

Yang Y, Zeng Z, Zhang C, Huang D, Zeng G, Xiao R, Lai C, Zhou C, Guo H, Xue W Construction of iodine vacancy-rich BiOI/Ag@AgI Z-scheme heterojunction photocatalysts for visible-light-driven tetracycline degradation: transformation pathways and mechanism insight Chem. Eng. J, 349 (2018a), pp. 808–821

Yang Y, Zhang C, Lai C, Zeng G, Huang D, Cheng M, Wang J, Chen F, Zhou C, Xiong W BiOX (X= Cl, Br, I) photocatalytic nanomaterials: applications for fuels and environmental management Adv. Colloid Interface Sci. (2018b)

Yao Y, Miao S, Liu S, Ma LP, Sun H, Wang Synthesis S, characterization, and adsorption properties of magnetic $Fe_3O_4$@ graphene nanocomposite Chem. Eng. J, 184 (2012), pp. 326–332

Yi H, Huang D, Zeng G, Lai C, Qin L, Cheng M, Ye S, Song B, Ren X, Guo X Selective prepared carbon nanomaterials for advanced photocatalytic application in environmental pollutant treatment and hydrogen production Appl. Catal., B (2018)

Yin W, Hao S, Cao H Solvothermal synthesis of magnetic CoFe2O4/rGO nanocomposites for highly efficient dye removal in wastewater RSC Adv., 7 (7) (2017), pp. 4062–4069

Zangeneh H, Zinatizadeh A, Habibi M, Akia M, Isa MH Photocatalytic oxidation of organic dyes and pollutants in wastewater using different modified titanium dioxides: a comparative review J. Ind. Eng. Chem, 26 (2015), pp. 1–36

Zhang DF, Zhang L Construction of a three-dimensional nest-like lithium ferrite/reduced graphene oxide composite with enhanced visible-light photocatalytic activity New J. Chem, 40 (8) (2016), pp. 7171–7180

Zhang YK, Yan LG, Xu WY, Guo XY, Cui LM, Gao L, Wei Q, Du B Adsorption of Pb(II) and Hg(II) from aqueous solution using magnetic CoFe2O4-reduced graphene oxide J. Mol. Liq, 191 (2014a), pp. 177–182

Zhang YK, Yan T, Yan LG, Guo XY, Cui LM, Wei Q, Du B Preparation of novel cobalt ferrite/chitosan grafted with graphene composite as effective adsorbents for mercury ions J. Mol. Liq, 198 (2014b), pp. 381–387

Zhou C, Xu P, Lai C, Zhang C, Zeng G, Huang D, Cheng M, Hu L, Xiong W, Wen X Rational design of graphic carbon nitride copolymers by molecular doping for visible-light-driven degradation of aqueous sulfamethazine and hydrogen evolution Chem. Eng. J, 359 (2019c), pp. 186–196

Zhou L, He B, Huang J One-step synthesis of robust amine-and vinyl-capped magnetic iron oxide nanoparticles for polymer grafting, dye adsorption, and catalysis ACS Appl. Mater. Interfaces, 5 (17) (2013), pp. 8678–8685 [PubMed: 23937378]

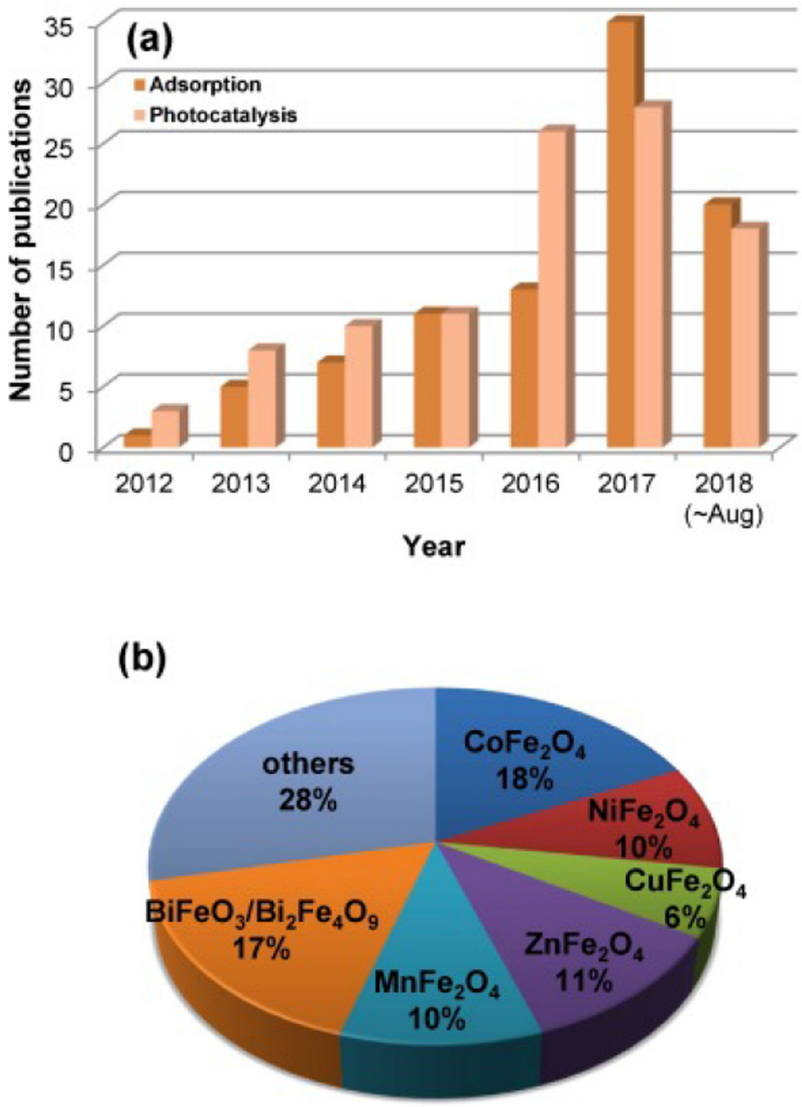


**Fig. 1.**

(a) Number of publications in the last six years (up to Aug. 2018) related to the use of GNSFs, obtained from Web of Science using the keywords “graphene”, “ferrite”, and “adsorption” or “photocatalysis”. (b) Percentage of references by the type of spinel ferrite.

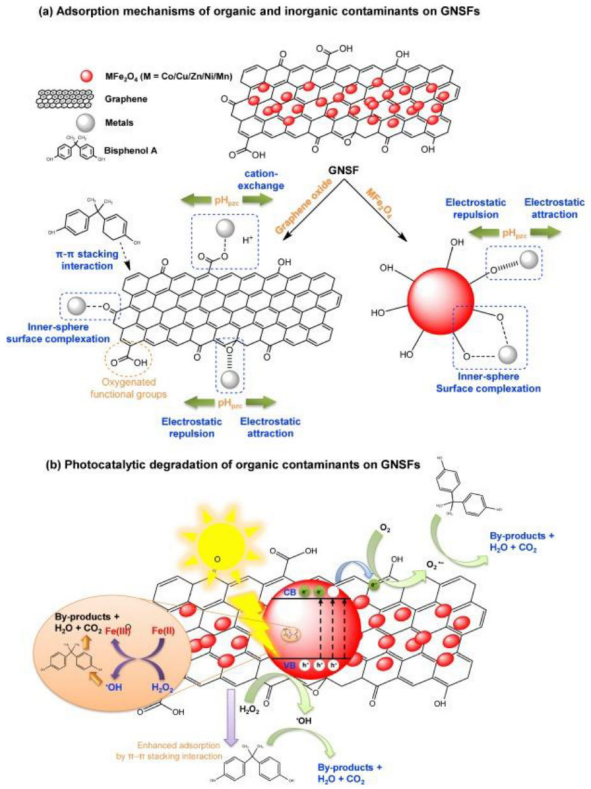


**Fig. 2.**

Schematic illustration of the mechanisms of the (a) adsorptive and (b) photocatalytic activities of GNSFs for contaminant removal.

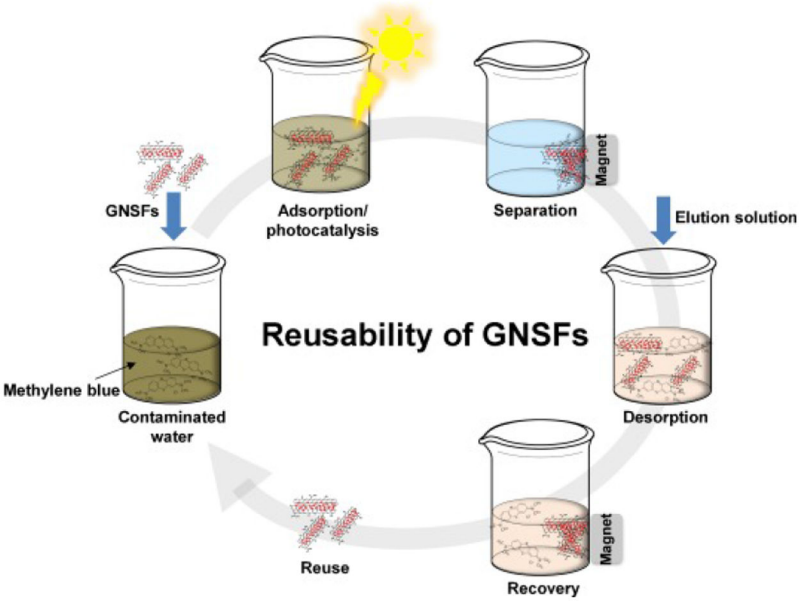


**Fig. 3.**

Schematic diagram illustrating contaminant adsorption/photocatalysis, desorption, recovery, and reuse process on the applications of GNSFs in aqueous solution.

**Table 1.**

GNSFs used for the removal of organic and inorganic contaminants from aqueous solutions and their adsorption capacity.

| Composite | Target contaminant* | Working conditions | | | | Maximum adsorption capacity (mg $g^{-1}$) | No. of cycles | Ref. |
|---|---|---|---|---|---|---|---|---|
| | | Dosage (g $L^{-1}$) | pH | Temp (K) | $C_0$ (mg $L^{-1}$) | | | |
| GO/$CuFe_2O_4$ on Fe__Ni foam | As(III)/As(V) | 8 | 7.2 | 323 | 10 | 51.6/125 | 9 | Wu et al. (2018) |
| rGO/$MnFe_2O_4$ | Glyphosate | 1 | – | 278–318 | 5–80 | 39 | – | Yamaguchi et al. (2016) |
| Graphene/$MnFe_2O_4$ | Pb(II)/Cd(II) | 0.025 | 2–8 | 300–320 | 10–70 | 100/76.9 | 3 | Chella et al. (2015) |
| $BFO_{249}$/$rGO_{4.5}$ | BPA | 0.5 | 6.5 | – | 10 | 4 | – | Hu et al. (2015a) |
| GO/$MnFe_2O_4$ | Pb(II)/As(III)/As(V) | 0.2 | – | 298–333 | 1–400 | 673/146/207 | 5 | Kumar et al. (2014) |
| Amino-functionalized GO/$SiO_2$@$CoFe_2O_4$ | ABI/Cr(VI) | 0.25–2 | 1–10 | 298 | 2.5–100 | 131/136 | 5 | Santhosh et al. (2017) |
| GO/$NiFe_2O_4$ | Pb(II)/Cr(III) | 0.75/0.5 | 5.5/4.0 | 298 | 0–25 | 25/45.5 | 4 | Lingamdinne et al. (2016b) |
| rGO/$CoFe_2O_4$/Polyaniline | U(VI) | 0.05 | 5 | 298 | 50 | 2430 | 8 | Dat et al. (2018) |
| rGO/$ZnFe_2O_4$ | MB | 1 | – | Ambient | 10 | 9.73 | 5 | Fei et al. (2016) |
| poly(m–phenylenediamine)/rGO (PmPD/rGO/NFO) | CR/MO/MB/Cr(VI) | 0.1 | 2–9 | Ambient | 100,000/20,000/20,000/20-250 | 286/137/103 | – | Wang et al. (2017b) |
| GO/$MnFe_2O_4$ | As(V) | 0.2 | 1–5 | – | 10–50 | 240 | 5 | Huong et al. (2016) |
| rGO/$Zn_{0.5}Ni_{0.5}Fe_2O_4$/polyaniline | U(VI) | 0.05 | 2–10 | 298 | 50 | 1885 | 5 | Tran et al. (2017) |
| GO/$MnFe_2O_4$ | La(III)/Ce(III) | 0.3 | 3–7 | 298–333 | 50–500 | 1001/982 | 3 | Ghobadi et al. (2018) |
| rGO/$NiFe_2O_4$ | U(VI)/Th(IV) | 0.3 | 3.5 | 293–333 | 2–30 | 200/127 | 5 | Lingamdinne et al. (2017a) |
| rGO/$CoFe_2O_4$ | Pb(II)/Hg(II) | 0.03–0.11 | 3–8 | 298–318 | 20/5 | 299/158 | – | Zhang et al. (2014a) |
| $CoFe_2O_4$–chitosan–graphene | Hg(II) | 0.01–0.12 | 2–7 | 323 | 20 | 361 | – | Zhang et al. (2014b) |
| rGO/gadolinium doped $ZnFe_2O_4$ (GZFG) | Levofloxacin | 0.12 | 6.5 | – | 5–60 | 14.81 | – | Naskar et al. (2018) |
| rGO/$NiFe_2O_4$ | Pb(II)/Cr(III) | 0.1–0.8 | 2–7 | 298–328 | 2–25 | 122/127 | 4 | Lingamdinne et al. (2017b) |
| Barium (II)–doped rGO/$ZnFe_2O_4$ ($Ba^{2+}$–ZF/rGO) | MB | 1 | – | – | 10–30 | 9.99 | 5 | Fei et al. (2017) |
| rGO/$CoFe_2O_4$ | U(VI) | 0.4 | 6.0 | 298–328 | – | 227 | – | Tan et al. (2015) |
| GO/$MnFe_2O_4$ | MB/As(V) | 0.2 | 7/1-2 | 298 | 2-8/0-50 | 177/240 | 5 | Huong et al. (2018) |
| 1,6–hexanediamine-functionalized rGO/$ZnFe_2O_4$ | Cr(VI) | 0.2 | 1–11 | 298 | 50–300 | 172 | 5 | Li et al. (2015) |
| rGO/$NiFe_2O_4$ | As(III)/As(V) | 0.3 | 6.5 | 283–323 | 7 | 65.8/106 | 6 | Lingamdinne et al. (2016a) |

| Composite | Target contaminant* | Working conditions | | | $C_0$ (mg $L^{-1}$) | Maximum adsorption capacity (mg $g^{-1}$) | No. of cycles | Ref. |
|---|---|---|---|---|---|---|---|---|
| | | Dosage (g $L^{-1}$) | pH | Temp (K) | | | | |
| $CoFe_2O_4$–G | Pb(II)/Cd(II) | 0.025 | 2–8 | 310 | 20 | 143/105 | 3 | Santhosh et al. (2015) |
| $NiFe_2O_4$–G | Pb(II)/Cd(II) | 0.025 | 2–8 | 310 | 20 | 111/75 | 3 | Santhosh et al. (2015) |
| rGO/$CoFe_2O_4$ | RhB/MB/CR/MG | 0.13–0.25 | 7 | 298–323 | 0.3 | 122/93.5/105/88.3 | 6 | Yin et al. (2017) |

ABI = Acid Black I; MG = Methylene Green.

**Table 2.**

Application of GNSFs for photocatalytic removal of organic contaminants from aqueous solutions.

| Composite | Target contaminant | Working conditions | | | | Removal capacity | No. of cycles | Ref. |
|---|---|---|---|---|---|---|---|---|
| | | Dosage (g $L^{-1}$) | pH | Temp (K) | $C_0$ (mg $L^{-1}$) | | | |
| Graphene–wrapped $Bi_2Fe_4O_9$/Ag | MB | 0.12 | ~6.5 | NA | NA | ~99% | 3 | Hu et al. (2015b) |
| N-doped graphene/ $NiFe_2O_4$ | MB | 0.25 | NA | 298 | 20 | >99% | NA | Singh et al. (2017) |
| graphene/$AgFeO_2$ | RhB/MB/MO | 5 | NA | 298 | 20 | >99/100/96% | 10 | Hosseini et al. (2017) |
| rGO/$ZnFe_2O_4$ | $NH_3/N_2$ | 2 | 9.5 | 298 | 100 | 92.4% | 5 | Liu et al. (2017) |
| $BFO_{249}$/$rGO_{4.5}$ | BPA | 0.5 | 6.5/5 | NA | 10 | 76/80% | NA | Hu et al. (2015a) |
| rGO/$CoFe_2O_4$ | MB/MO/RhB | 0.25 | NA | 298 | 20 | >93/37.5/72.2% | 3 | He et al. (2015) |
| rGO/$NiFe_2O_4$ | MB/MO/RhB | 0.25 | NA | 298 | 20 | 99.1/47.1/82.2% | 3 | Liang et al. (2018) |
| rGO/$CoFe_2O_4$ | 4-CP | 0.4 | NA | 318 | 10 | >99% | 3 | Devi and Srinivas (2017) |
| Chitosan/GO/$CoFe_2O_4$ | Maxilon C.I. basic dye | 2 | NA | 303 | 25 | 99% | 4 | (Al-Kahtani and Abou Taleb, 2016) |
| $C_3N_4$@$MnFe_2O_4$-G | MNZ/TC | 1 | NA | NA | 10–20 | 94.5/91.5% | 5 | Wang et al. (2017c) |
| Graphene-based–$CoFe_2O_4$/CdS | MB | 0.25 | NA | 298 | 20 | 80% | 3 | Shi et al. (2014) |
| rGO/$TiO_2$/$CoFe_2O_4$ | MO | 0.25 | NA | NA | 20 | >99% | 5 | Ghosh et al. (2017) |
| Nest-like rGO/$LiFe_5O_8$ | MB | 1 | 6.4 | NA | 10 | 99.6% | 4 | Zhang and Zhang (2016) |
| rGO/$ZnFe_2O_4$ | MB | 0.5 | NA | 308 | 10 | 99.23% | 9 | Rani et al. (2017) |
| rGO/$CoFe_2O_4$ | MO | 0.5 | NA | NA | 20 | >99% | 5 | Moitra et al. (2016) |
| rGO/$MnFe_2O_4$ | MB | 0.5 | NA | 298 | 50 | 95% | 4 | Peng et al. (2016) |

TC: tetracycline; NA: not available.